First principles kinetic-collective thermal conductivity of semiconductors

P. Torres,[1] A. Torelló,[1] J. Bafaluy,[1] J. Camacho,[1] X. Cartoixà,[2] and F. X. Alvarez[1,*]
[1]*Departament de Física, Universitat Autònoma de Barcelona, 08193 Bellaterra, Catalonia, Spain*
[2]*Departament d'Enginyeria Electrònica, Universitat Autònoma de Barcelona, 08193 Bellaterra, Catalonia, Spain*
(Received 20 May 2016; revised manuscript received 7 March 2017; published 7 April 2017)

A fully predictive kinetic-collective model using *first principles* phonon spectra and relaxation times is presented. Thermal conductivity values obtained for Si, Ge, C (diamond), and GaAs in a wide range of sizes and temperatures are in good agreement with experimental data without the use of any fitting parameter. These results open the door to discuss how the precise combination of kinetic and collective contributions to heat transport could provide a useful framework to interpret recent complex experiments displaying non-Fourier behavior.

DOI: 10.1103/PhysRevB.95.165407

I. INTRODUCTION

Recent experiments of thermal transport in semiconductors since the appearance of ultrafast laser techniques, measuring the effective thermal conductivity using heaters with different sizes and working in different excitation frequency ranges, have shown that the Fourier law breaks down at reduced size and time scales [1–7]. To understand the origin of this new behavior, the authors try to obtain the thermal conductivity spectral distribution (TCSD) in terms of the phonon relaxation times or the phonon mean free paths (MFP) [2–9].

To extract the TCSD from experiments, a microscopic insight is needed. In the standard kinetic framework, thermal conductivity is obtained by adding independent single mode contributions [6]. This approach is known to be valid for highly resistive materials at large size scales. Although normal scattering (N scattering) does not directly contribute to the thermal resistivity, it can cause qualitative differences in heat flow [10,11]: Momentum conservation does not allow a rapid relaxation of thermal disturbances, and heat flux can change to a regime where phonons are highly correlated (collective regime) [12]. In this case the contribution of the participating modes to the total thermal transport can change dramatically [13]. Several works have focused on obtaining a proper framework to address the effect of N scattering, either iteratively solving the Boltzmann transport equation (BTE) [14–16] or keeping the kinetic description and changing to a different quasiparticle like relaxons [17]. Another approach is the kinetic-collective model (KCM), derived from the solution to the Boltzmann transport equation (BTE) [12] expanded in terms of eigenstates of the N collision operator [18]. Thus, the KCM is a natural framework to understand and analyze systems where phenomena related to momentum conservation are expected to be important, such as graphene [15,19] or light group IV semiconductors [20].

The purpose of this work is to show that the KCM provides a useful framework to describe heat transport at all length scales. On one hand, KCM in combination with *first principles* calculations of harmonic and anharmonic interatomic force constants (IFC) is able to predict the thermal conductivity of a wide range of semiconductor samples from bulk to nanoscale without using any fitting parameter. On the other hand, we argue that differences between the kinetic and collective contributions to heat transport can be important to interpret recent results in ultrafast heating experiments as size and temperature change.

II. THE KINETIC-COLLECTIVE MODEL

According to the KCM not all the energy is carried kinetically by independent collisions, but part of this energy is carried by collective modes, which have their origin in N collisions. The collective behavior appears as a result of a coupling of modes generated through N processes. As a consequence, phonons of different modes perform as a whole resistive (R) collision, therefore all modes share the same collision mean free time (MFT), the so-called collective MFT, τ_c. A complete description of the model can be obtained elsewhere [12,20,21]. The thermal conductivity thus can be split into a kinetic and a collective contribution weighed by a switching factor $\Sigma \in [0,1]$ measuring the relative importance of the N and R scattering through the relaxation times, τ_N and τ_{RB}, where the latter refers to R processes including boundary scattering. In contrast to the kinetic contribution, where every mode has its own MFT, τ_k, the collective contribution is characterized by the same MFT for all modes, τ_c. In addition, the boundary effects are treated differently in the two contributions. While boundary scattering τ_B is included through the Mathiessen rule in the kinetic contribution, a form factor F, determined by the sample geometry alone through an effective length L_{eff}, describes size effects in the collective term. Thus, in the calculation of τ_c only Umklapp (U) and impurity scattering processes are considered. In bulk materials $\tau_B \to \infty$ and, $F = 1$, then the thermal conductivity only depends on intrinsic scattering events. The KCM equations are the following:

$$\kappa = \kappa_k + \kappa_c \,, \tag{1}$$

$$\kappa_k = (1-\Sigma)\int \hbar\omega \frac{\partial f}{\partial T} v^2 \tau_k D d\omega \,, \tag{2}$$

$$\kappa_c = \Sigma F \int \hbar\omega \frac{\partial f}{\partial T} v^2 \tau_c D d\omega \,, \tag{3}$$

$$\Sigma = \frac{1}{1+\frac{\tau_N}{\tau_{RB}}} \,, \tag{4}$$

*xavier.alvarez@uab.cat

where $\kappa_k(L_{\rm eff},T)$ and $\kappa_c(L_{\rm eff},T)$ are the kinetic and collective contributions, respectively, f is the Bose-Einstein distribution function, $v(\omega)$ the mode velocity, and $D(\omega)$ the density of states (DOS) of each mode. Notice that N scattering does not play any resistive role, but just weigh the contribution of each regime through the switching factor $\Sigma(L_{\rm eff},T)$. When R collisions are dominant, $\tau_{RB} \ll \tau_N$, one has $\Sigma \to 0$ and only the kinetic mechanism is at play. When τ_N becomes comparable to τ_{RB} both contributions are at work. The Appendix supplies the explicit expressions for the calculation of $\tau_k(L_{\rm eff},T,\omega)$, $\tau_c(T)$, $\tau_N(T)$, $\tau_{RB}(L_{\rm eff},T)$, and $F(L_{\rm eff},T)$ provided by the KCM.

III. FIRST PRINCIPLES CALCULATIONS

All the needed magnitudes in Eqs. (1)–(4) are calculated from *first principles* using the QUANTUM ESPRESSO package [22], which implements density functional theory (DFT) [23,24] under the local density approximation in the parametrization of Perdew and Zunger [25]. Core electrons were accounted for with norm-conserving pseudopotentials of the Von Barth-Car type [26,27]. Plane waves were cut off at an energy of 60 Hartree and Born effective charges and dielectric tensor were employed for GaAs to account for its polar behavior. Finally, small atomic cartesian displacements in a $3 \times 3 \times 3$ supercell with 216 atoms up to third neighbours were performed to compute second and third order force constants. A $20 \times 20 \times 20$ q-point grid is used for phonon Brillouin zone sampling in such calculations, while a $160 \times 160 \times 160$ mesh is used for the DOS calculations. N and U phonon relaxation times are obtained through the anharmonic IFC. For this the open code package ALAMODE [28] is used, where splitting of N and U events has been manually implemented in the code. Extrapolation of the latter values has been done for low frequencies in the DOS mesh sampling.

For the boundary collision rates in the kinetic contribution we use the Casimir expression [29] $\tau_B = L_{\rm eff}/v$, where $L_{\rm eff} = d_{\rm wire}$ is the wire diameter, $L_{\rm eff} = 2.25h$ for thin films, with h the film thickness, and $L_{\rm eff} = 1.12\sqrt{A}$ for square rods of cross section A [12].

For the impurity collision rate, we use Tamura's expression [30,31]

$$\tau_I^{-1} = \frac{\pi}{6}\Gamma\omega^2 D, \tag{5}$$

where Γ is the mass variance of the sample depending on the isotopic abundance of the sample. Notice that all these magnitudes are calculated and no free parameters are used.

Figure 1 represents the obtained frequency dependent phonon relaxation times for all the considered scattering mechanisms in a 2.8 mm bulk Si sample (the N and U scattering curves correspond to binning of the points from the inset in Fig. 1). At low frequencies, in the interval from 1.6×10^{-7} THz to 0.75 THz, we use theoretically derived expressions as follows. We employ Han's expressions [32] for the U processes, providing a transition from $\tau_U^{-1} \propto \omega^3$ to $\tau_U^{-1} \propto \omega^2$. For N processes, Herring's expression [33] where $\tau_N^{-1} \propto \omega^2 T^3$ is used. Using analytical expressions for low frequencies, accurate results can be achieved even with a coarse q-point grid to compute the scattering rates.

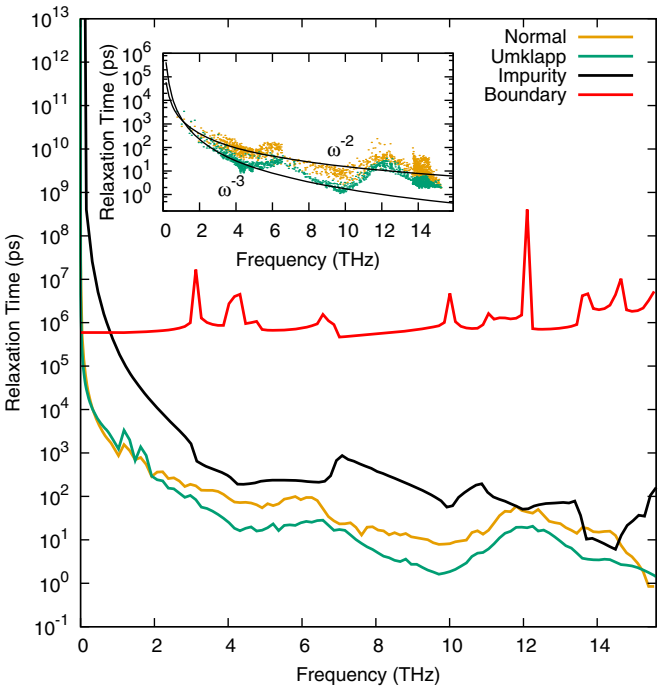

FIG. 1. Impurity, boundary, normal, and Umklapp relaxation times for 2.8 mm silicon rod in terms of frequency at $T = 300$ K. Impurity is obtained with Eq. (5), the boundary curve following Ref. [29], and Umklapp and normal curves are calculated averaging the *ab initio* results over bins. Raw *ab initio* data are plotted in the inset together with the analytic approximations.

IV. THERMAL CONDUCTIVITY PREDICTIONS

The calculated thermal conductivities of KCM compared to experimental measurements for bulk Si, Ge, diamond, and GaAs samples in a range of temperatures are plotted in Fig. 2 top. The good agreement between predictions and experiments without any adjustable parameter shows that the model is set on solid grounds. Similar results for bulk samples have also been obtained using a different approach based on an iterative solution of the BTE [14]. In the latter approach, the effect of the N processes is included through the iterative process, whereas in KCM this is determined by Σ. Thermal conductivity predictions of several bulk samples like silicon or germanium can also be obtained under relaxation time approximation (RTA). However, in this approach N processes are not correctly included [10,11], since they are treated as resistive processes. As a consequence, in samples where N scattering is important, like diamond or graphene, RTA underestimates the thermal conductivity [16].

Figure 2 bottom shows the KCM predictions of the thermal conductivity for nanowires and films. Good predictions are obtained for both kind of samples at sizes bigger than $L_{\rm eff} = 50$ nm. The strong reduction observed in the experimental data of the 22 nm NW could be associated with an enhancement of the boundary effects due to the high roughness of the surface. This effect is not captured in the simple diffuse model used in the present paper. Let us note that comparison to experimental data for silicon nanowires using a parameter free approach as a function of temperature and size has not been previously

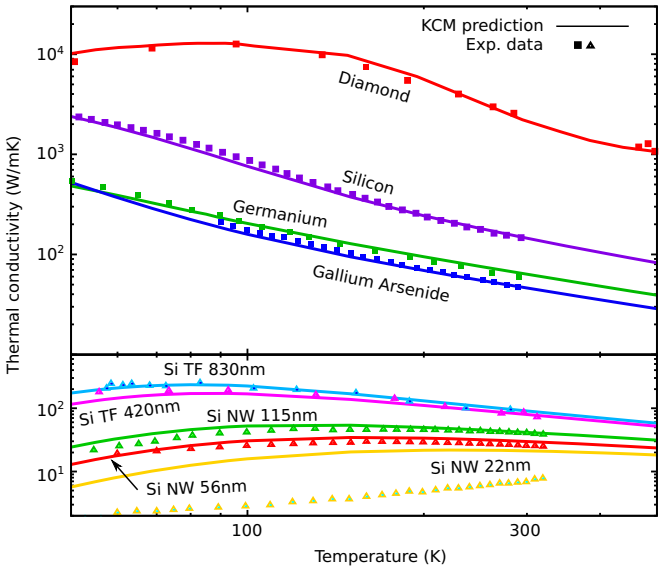

FIG. 2. Top: KCM prediction of thermal conductivity for bulk Si, Ge, diamond, and GaAs from Eqs. (1)–(4) using *ab initio* scattering rates compared to experimental data. Bottom: KCM predictions of thermal conductivity for thin films and nanowires. Points represent experimental data from Refs. [34,44–46] for bulk and from Refs. [35,42,43] for nano/micro samples. Lines describe the theoretical predictions.

published. In the case of thin films, good predictions have been obtained in previous works as a function of size [36]. Some N-as-resistive based descriptions like RTA have also provided good fits to data at the nanoscale by including a form factor and by using different isotope relaxation times from the ones corresponding to bulk [37,38]. In contrast, KCM uses a diffuse scattering model in the kinetic regime and a form factor F in the collective one accounting for boundary effects. This allows KCM to make nanoscale predictions without modifying bulk parameters. In this case, the form factor F is derived ensuring the conservation of energy and momentum of the whole phonon distribution [21,39], in contrast to form factors derived from N-as-resistive standpoints.

Figure 3 compares thermal conductivity predictions for bulk natural diamond and a 56 nm silicon nanowire in KCM and RTA. For bulk diamond, the importance of N processes makes RTA to underestimate the thermal conductivity, as reported by Li *et al.* [16,40] and Ward *et al.* [41] for isotopically enriched diamond. On the other side, RTA with a simple diffuse boundary scattering model [29] overestimates the experimental data for small wire diameters. The KCM, that properly accounts for N processes and boundary effects in both transport regimes (kinetic and collective), is able to correctly predict the thermal conductivity in a simple way in both cases.

Figure 4 presents KCM calculations of the thermal conductivity from bulk to 22 nm wires at 300 K and a comparison to RTA and iterative BTE predictions [16]. KCM provides good predictions without any fitting parameter for wires as small as 56 nm. The overprediction of the smallest wires, as seen in Fig. 2 bottom, could be associated with an increased roughness effect [38,47]. This behavior has also been observed for thin films at similar scales [36]. The green zone in Fig. 4 displays

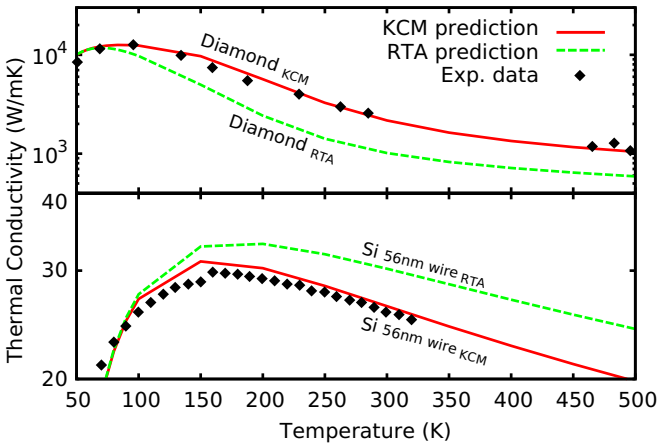

FIG. 3. Comparison of KCM and RTA predictions for bulk natural diamond (top) and 56 nm Si nanowire (bottom). Experimental data (symbols) are taken from Refs. [42,46].

the kinetic contribution to thermal conductivity, namely κ_k. The difference between the black line and the green zone is the collective contribution (red zone), κ_c. While the agreement to data using only kinetic transport is good for the smallest diameters (where the red zone vanishes), for bigger sizes and bulk the collective contribution is required. It is thus the right combination of kinetic and collective contributions as expressed by Eqs. (1)–(4) that yields good predictions in the whole size range.

V. COLLECTIVE BEHAVIOR

As indicated above, the relative weight of collective and kinetic transport included in the value of the switching factor Σ could be the reason behind the previous difficulties to consistently predict the thermal conductivity at all sizes and temperatures. Thus, the dependence of Σ on those magnitudes

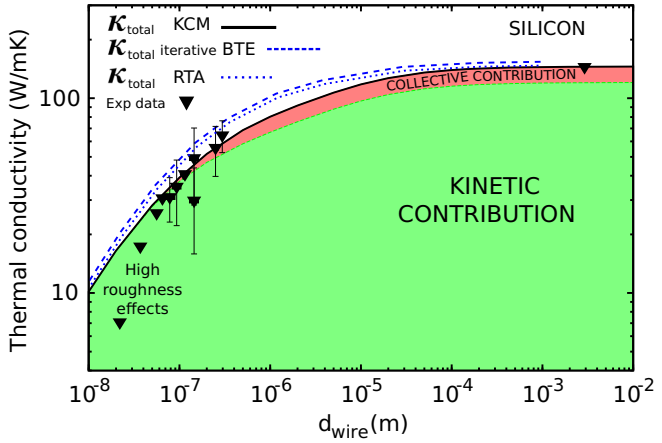

FIG. 4. Theoretical predictions and experimental data for thermal conductivity of silicon wires at $T = 300$ K as a function of the wire diameter. Kinetic (green), collective (red), and total thermal conductivity predicted by KCM (black solid line), RTA (blue dot), and iterative BTE predictions from Ref. [16] (blue dashed line). Experimental data (symbols) are taken from Refs. [42,43,45].

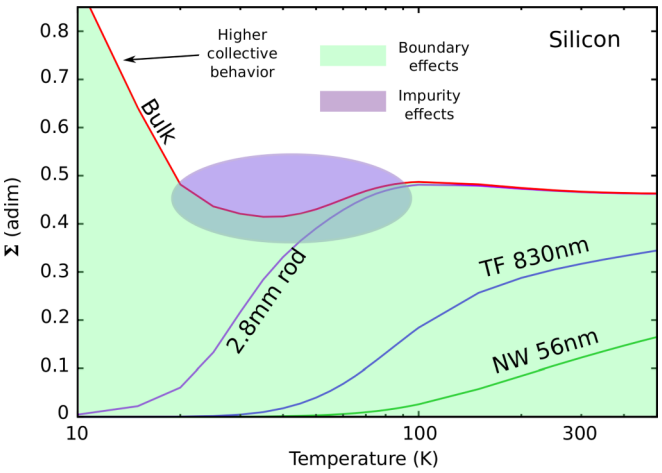

FIG. 5. Switching factor Σ for bulk silicon, 2.8 mm rod, 830 nm film, and 56 nm wire as a function of temperature. The purple region indicates the effect of the impurity scattering.

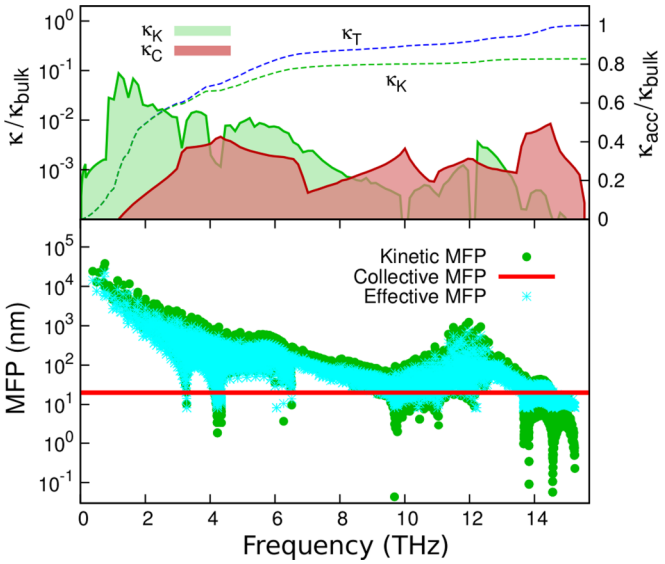

FIG. 6. Top: Thermal conductivity spectral distribution (TCSD) in terms of frequency for bulk silicon at $T = 300$ K. Filled curves are the kinetic and collective contributions to TCSD. Blue line represents the total thermal conductivity accumulation function (TCAF), that is, the integral of TCSD. The green line represents the accumulated kinetic thermal conductivity, thus the difference between both is the collective contribution. Bottom: Mode kinetic and collective MFP in terms of frequency.

could be key to interpret experiments at different temperatures and sizes [2,48]. Indeed, the collective contribution, which is the contribution to heat transport due to momentum conservation, is probably responsible for the hydrodynamic behavior proposed recently to describe thermal conduction in recent works [15,19]. Then, we expect hydrodynamic effects to be relevant for finite values of Σ.

The dependence of Σ on size and temperature can be directly obtained by examining how R and N processes change as those parameters are modified. Since we have introduced the boundary scattering τ_B in the resistive term τ_{RB}, as size is reduced, the rate of boundary collisions increases (and so the resistive collision rates), meanwhile N scattering rates do not change. As a result, as size is reduced R collisions become dominant and the parameter Σ tends to zero. This explains the convergence of κ_{tot} to κ_k for small samples displayed in Fig. 4. Figure 5 shows the value of Σ, as defined in Eq. (4), for 2.8 mm silicon rod, 830 nm thin film, and 56 nm nanowire in terms of temperature. The observed reduction of Σ as temperature decreases has the same origin: At low temperatures, anharmonicities become less important in front of boundary and impurity scattering rates, which are temperature independent, and this reduces the collective contribution. At high temperatures, Σ increases in all cases tending to a constant value.

Figure 5 also includes the bulk value Σ_{bulk} that represents the intrinsic collective behavior for silicon at 300 K. From this representation it can be observed that when no boundaries are considered the collective behavior becomes more important as the temperature decreases. This increase is due to the fact that at low temperatures, although anharmonicities decrease, the N scattering is dominant in front of U processes. In recent theoretical works the appearance of a hydrodynamic behavior at low temperatures has been reported in 2D materials like graphene [15,19], in agreement with the behavior predicted by Σ_{bulk}. It is expected that when materials intrinsically exhibit collective behavior, as found in silicon, hydrodynamic heat flux equations can be used with suitable boundary conditions to compute the thermal conductivity as a function of temperature and size [18].

VI. THERMAL CONDUCTIVITY SPECTRAL DISTRIBUTION

In the last years, several works have pointed out the importance of long MFP (i.e., low frequency) phonons in thermal conductivity. It is widely accepted that these phonons have a very important contribution to heat transport, but current DFT calculations seem to provide larger contributions of long MFP phonons than experimental observations [49,50]. To be able to predict correctly the thermal conductivity from such *ab initio* calculations, Akhiezer damping has been proposed. This macroscopic relaxation mechanism has been phenomenologically used to reduce the *first principles* obtained MFT as an extra scattering mechanism in the Mathiessen rule [50]. KCM may provide an alternative explanation for the reduction in the contribution of low frequency phonons to thermal conductivity based on the effects of the collective regime and on the calculation of low energy relaxation times.

Figure 6 top displays the kinetic and collective TCSD predicted by KCM for bulk silicon as a function of frequency at 300 K, where one observes that both contributions span the whole range of the spectrum. While at low frequencies the kinetic regime dominates, the collective contribution becomes more important at high frequencies. A direct correspondence with the MFP spectral distribution (Fig. 6 bottom) can be done through this representation.

Figure 6 bottom shows the MFP in terms of frequency for the kinetic and collective terms. From the KCM, $\ell_k(\omega) = v\tau_k$ is the kinetic MFP, and $\ell_c(T) = \bar{v}\tau_c$ is the collective MFP,

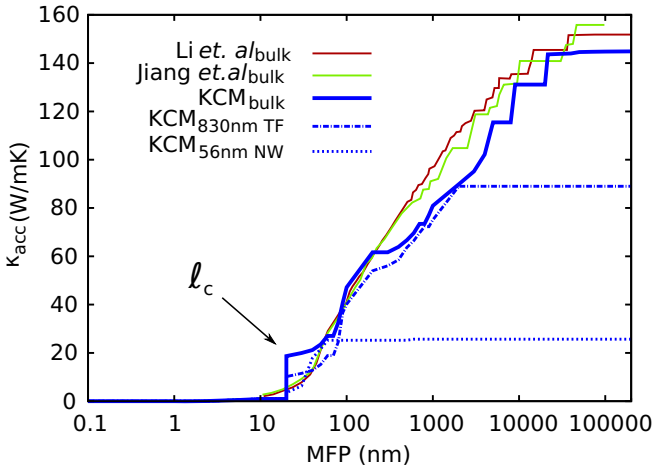

FIG. 7. TCAF in terms of MFP for bulk silicon at $T = 300$ K in KCM compared to that of Li *et al.* [16] and Jiang *et al.* [50]. KCM predictions for 830 nm film and 56 nm wire are also included.

where

$$\bar{v} = \frac{\int v\,\hbar\omega\frac{\partial f}{\partial T}Dd\omega}{\int \hbar\omega\frac{\partial f}{\partial T}Dd\omega} \tag{6}$$

is the mean phonon velocity (independent of ω). It is important to notice that while the kinetic MFP is different for all the modes, the collective MFP is the same for all of them. An effective MFP (blue asterisk) has been included to show the effect of the collective phonons from a pure kinetic point of view, where $\ell_{eff}(\omega) = (1-\Sigma)\ell_k(\omega) + \Sigma\ell_c$. From this representation one can appreciate a reduction of the MFP of long MFP phonons at low frequencies and an increase for the smaller ones at high frequencies [13]. This effect of the collective regime is a consequence of the energy and momentum conservation of the whole distribution introduced through Σ [21].

In Fig. 7 the accumulated thermal conductivity in terms of MFP for bulk silicon at 300 K is represented to show the differences between KCM and current kinetic models. It can be observed that in the KCM the largest MFP phonon that contributes to κ is $\ell_k \sim 20$ μm, in agreement with experimental observations [50]. This is due to the fact that for low frequency phonons, the use of Han's expressions [32] provides a $\tau_U^{-1} \propto \omega^2$ dependence for the U processes instead of the widely used approximation $\tau_U^{-1} \propto \omega^3$. Note that the use of an analytical expression allows us to avoid the over/underestimations provided by DFT calculations at these frequency ranges [49]. Differences on the slope of κ_{acc} between 100 nm and 10 μm in the KCM have its origin in that N scattering does not appear in the integral expressions of resistive terms.

A characteristic feature of the KCM accumulation function is the appearance of a step at the collective MFP, ℓ_c. From Fig. 7 it can be seen that while the kinetic contribution spans all the distribution the collective one occurs only at a fixed MFP, $\ell_c \sim 20$ nm for natural silicon at 300 K. The height of this step is proportional to the value of Σ and, as the switching factor depends on the size of the sample, it will be different for each L_{eff}, according to Fig. 5. Comparing the curves for different sizes (56 nm nanowire, 830 nm thin film, and bulk) in Fig. 7 one can conclude that the TCAF of a sample cannot be obtained by just removing from the bulk curve the contribution of phonons with MFP larger than its characteristic length L_{eff} [36].

The position of the step at ℓ_c in the thermal conductivity accumulation function (TCAF) can be related to a characteristic nonlocal scale $\ell = \sqrt{\ell_c \ell_N/5}$ that is associated with hydrodynamic effects like Poiseuille flow or second sound, where $\ell_N = \bar{v}\tau_N$ is the normal MFP [21]. A direct detection of this step would be difficult for small samples because at these scales Σ is small. From our calculations the nonlocal scale for silicon at 300 K is $\ell \sim 100$ nm. Recent experiments carried out on bulk silicon by Hoogeboom-Pot *et. al* [7] show that collective effects appear when characteristic scales of the order of 10^2 nm are considered in the experiment, in agreement with the obtained nonlocal length ℓ. It is important to remark that the consequences of collective effects on the measured thermal conductivity will depend on each experimental setup.

VII. CONCLUSIONS

We have introduced the collective behavior as a fundamental piece to understand thermal conductivity when normal scattering plays an important role. This new transport mechanism is combined with the kinetic transport in the KCM, providing a way to calculate the thermal conductivity without treating normal scattering as a resistive mechanism, in contrast to N-as-resistive approaches like RTA. By using *first principles* calculations, we have seen that KCM provides good agreement with experimental data for a number of samples without free parameters. They include several bulk materials and micro/nano silicon films and wires in a wide range of temperatures. While thermal conductivity of some samples can be predicted by RTA, KCM additionally provides good predictions for bulk diamond and silicon nanowires thanks to the correct treatment of normal processes and the form factor used in the collective regime.

The importance of collective behavior in a specific sample is determined by the parameter Σ, calculated from the ratio of normal to resistive scattering times. As boundary scattering is included in the resistive term, when size is reduced $\Sigma \to 0$, and Σ also vanishes at low temperatures. In bulk samples, where boundaries are not considered, the collective behavior is relevant at all temperatures, becoming more important as temperature decreases. Since the collective regime is expected to be responsible for the appearance of hydrodynamic effects, for finite values of Σ hydrodynamic equations can be used to study heat transport.

In the last years the role of low energy phonons has been demonstrated to be important in order to compute the thermal conductivity and to analyze the thermal conductivity accumulation function in terms of mean free path. KCM supplies an explanation for the reduction of the contribution of long mean free paths phonons based on the effect of the collective regime and the calculation of low frequency relaxation times. In addition, in the KCM accumulation function the emergence of a collective characteristic length provides information of the scales where deviations from Fourier will be relevant, which are not visible from classical representations. Finally, the dependence of Σ on the characteristic size L_{eff} changes the

shape of this function, and therefore the general belief that the thermal conductivity for a certain size L_{eff} can be obtained by removing the contribution from phonons with mean free path greater than it.

In summary, the collective regime defined in KCM introduces relevant information on phonon transport that could be useful to describe experiments where non-Fourier behavior has been reported, as in high temperature gradients or ultrafast experiments using pump-probe and/or thermoreflectance setups.

ACKNOWLEDGMENTS

We acknowledge fruitful discussions with Dr. R. Rurali. We also acknowledge the financial support of the Spanish Ministerio de Economia y Competitividad under Grant Consolider nanoTHERM CSD2010-00044, TEC2015-67462-C2-2-R (MINECO/FEDER), TEC2015-67462-C2-1-R (MINECO/FEDER).

APPENDIX

In this appendix we supply explicit expressions for the parameters τ_c, τ_N, τ_{RB}, and F used in Eqs. (1)–(4). A derivation of these equations from the Boltzmann transport equation can be obtained in the original manuscript of Guyer and Krumhansl [18], which has been used recently for the specific case of graphene [15]. For the sake of simplicity, we express the different projections of the phonon distribution function in the momentum space found in these equations in terms of function $C_i(\omega)$ defined as:

$$C_i(\omega) = \left(\frac{v|q|)}{\omega}\right)^{2i} \hbar\omega \frac{\partial f}{\partial T} D \,, \tag{A1}$$

where $v(\omega)$ denotes the phonon mode velocity and $|q(\omega)|$ is the modulus wave vector. Note that C_0 directly represents the specific heat of mode ω.

The kinetic contribution is

$$\kappa_k(L_{\text{eff}},T) = (1-\Sigma)\int C_0 v^2 \tau_k d\omega, \tag{A2}$$

where

$$\tau_k^{-1}(L_{\text{eff}},\omega,T) = \tau_B^{-1} + \tau_{int}^{-1} \tag{A3}$$

is the total kinetic relaxation time. This is calculated with the Mathiessen rule combining the boundary scattering time $\tau_B(L_{\text{eff}},\omega)$ and the intrinsic relaxation time:

$$\tau_{\text{int}}^{-1}(\omega,T) = \tau_I^{-1} + \tau_U^{-1} \,, \tag{A4}$$

where $\tau_I(\omega)$ and $\tau_U(\omega,T)$ are the impurity and Umklapp relaxation times, respectively.

The collective contribution is

$$\kappa_c(L_{\text{eff}},T) = \Sigma F \int C_0 v^2 \tau_c d\omega \,, \tag{A5}$$

where the collective mean free time is an average over the whole distribution obtained as

$$\tau_c(T) = \frac{\int C_1 d\omega}{\int \frac{1}{\tau_{\text{int}}} C_1 d\omega} \,. \tag{A6}$$

Notice that in the collective mean free time boundary scattering is not included, but only intrinsic scattering rates are used. The form factor F for a generalized geometry can be approximated by [39]

$$F(L_{\text{eff}}) = \frac{1}{2\pi^2}\frac{L_{\text{eff}}^2}{\ell^2}\left(\sqrt{1+4\pi^2\frac{\ell^2}{L_{\text{eff}}^2}}-1\right), \tag{A7}$$

where L_{eff} is the effective length of the sample depending on its geometry and ℓ the characteristic nonlocal scale [21] defined in the main paper.

The switching factor Σ [Eq. (4)] that determines the relative importance of the kinetic and collective contributions and ensures the momentum conservation [21] depends on the integrated R and N scattering mean free times, τ_{RB} and τ_N. Their expressions are:

$$\tau_{RB}(L_{\text{eff}},T) = \frac{\int C_1 \tau_k d\omega}{\int C_1 d\omega} \tag{A8}$$

and

$$\tau_N(T) = \frac{\int C_0 \tau_N d\omega}{\int C_0 d\omega} \,. \tag{A9}$$

Note that the resistive mean free time, τ_{RB}, as given in Eq. (A8) depends on L_{eff} through the boundary scattering rate in τ_k. From the definition of these time constants, let us remark that, if phonon scattering is only due to normal collisions, the thermal conductivity predicted by KCM goes to infinity, as it should, since τ_k and τ_c diverge.

[1] M. E. Siemens, Q. Li, R. Yang, K. K. A. Nelson, E. H. Anderson, M. M. Murnane, and H. C. Kapteyn, Nat. Mater. Lett. **9**, 26 (2010).
[2] A. J. Minnich, J. A. Johnson, A. J. Schmidt, K. Esfarjani, M. S. Dresselhaus, K. A. Nelson, and G. Chen, Phys. Rev. Lett. **107**, 095901 (2011).
[3] K. T. Regner, D. P. Sellan, Z. Su, C. H. Amon, A. J. H. McGaughey, and J. Malen, Nat. Commun. **4**, 1640 (2013).
[4] J. A. Johnson, A. A. Maznev, J. Cuffe, J. K. Eliason, A. J. Minnich, T. Kehoe, C. M. S. Torres, G. Chen, and K. A. Nelson, Phys. Rev. Lett. **110**, 025901 (2013).
[5] R. B. Wilson and D. G. Cahill, Nat. Commun. **5**, 5075 (2014).
[6] Y. Hu, L. Zeng, A. J. Minnich, M. S. Dresselhaus, and G. Chen, Nat. Nanotechnol. **10**, 701 (2015).
[7] K. M. Hoogeboom-Pot, J. N. Hernandez-Charpak, E. H. Anderson, X. Gu, R. Yang, M. M. Murnane, H. C. Kapteyn, and D. Nard, Proc. Natl. Acad. Sci. **112**, 4846 (2015).
[8] A. M. S. Mohammed, Y. R. Koh, B. Vermeersch, H. Lu, P. G. Burke, A. C. Gossard, and A. Shakouri, Nano Lett. **15**, 4269 (2015).
[9] B. Vermeersch, J. Carrete, N. Mingo, and A. Shakouri, Phys. Rev. B **91**, 085202 (2015).

[10] R. E. Peierls, *Quantum Theory of Solids* (Oxford University Press, Oxford, 2007).
[11] J. M. Ziman, *Electrons and Phonons: The Theory of Transport Phenomena in Solids* (Oxford University Press, Oxford, 2001).
[12] C. De Tomas, A. Cantarero, A. F. Lopeandia, and F. X. Alvarez, J. Appl. Phys. **115**, 164314 (2014).
[13] C. De Tomas, A. Cantarero, A. F. Lopeandia, and F. X. Alvarez, J. Appl. Phys. **118**, 134305 (2015).
[14] D. A. Broido, M. Malorny, G. Birner, N. Mingo, and D. A. Stewart, Appl. Phys. Lett. **91**, 231922 (2007).
[15] S. Lee, D. Broido, K. Esfarjani, and G. Chen, Nat. Commun. **6**, 6290 (2015).
[16] W. Li, N. Mingo, L. Lindsay, D. A. Broido, D. A. Stewart, and N. A. Katcho, Phys. Rev. B **85**, 195436 (2012).
[17] A. Cepellotti and N. Marzari, Phys. Rev. X **6**, 041013 (2016).
[18] R. A. Guyer and J. A. Krumhansl, Phys. Rev. **148**, 766 (1966).
[19] A. Cepellotti, G. Fugallo, L. Paulatto, M. Lazzeri, F. Mauri, and N. Marzari, Nat. Commun. **6**, 6400 (2015).
[20] C. de Tomas, A. Cantarero, A. F. Lopeandia, and F. X. Alvarez, Proc. R. Soc. London A **470**, 20140371 (2014).
[21] R. A. Guyer and J. A. Krumhansl, Phys. Rev. **148**, 778 (1966).
[22] P. Giannozzi, S. Baroni, N. Bonini, M. Calandra, R. Car, C. Cavazzoni, D. Ceresoli, G. L. Chiarotti, M. Cococcioni, I. Dabo *et al.*, J. Phys.: Condens. Matter **21**, 395502 (2009).
[23] P. Hohenberg and W. Kohn, Phys. Rev. **136**, B864 (1964).
[24] W. Kohn and L. J. Sham, Phys. Rev. **140**, A1133 (1965).
[25] J. P. Perdew and A. Zunger, Phys. Rev. B **23**, 5048 (1981).
[26] A. Fallis, Journal of Chemical Information and Modeling **53**, 1689 (2013).
[27] A. Dal Corso, S. Baroni, R. Resta, and S. de Gironcoli, Phys. Rev. B **47**, 3588 (1993).
[28] T. Tadano, Y. Gohda, and S. Tsuneyuki, J. Phys.: Condens. Matter **26**, 225402 (2014).
[29] H. Casimir, Physica **5**, 495 (1938).
[30] W. S. Capinski, H. J. Maris, and S. Tamura, Phys. Rev. B **59**, 10105 (1999).
[31] S. I. Tamura, Phys. Rev. B **27**, 858 (1983).
[32] Y. J. Han and P. G. Klemens, Phys. Rev. B **48**, 6033 (1993).
[33] C. Herring, Phys. Rev. **95**, 954 (1954).
[34] A. Inyushkin, A. Taldenkov, A. Yakubovsky, A. Markov, L. Moreno-Garsia, and B. Sharonov, Semicond. Sci. Technol. **18**, 685 (2003).
[35] M. Asheghi, M. Touzelbaev, K. Goodson, Y. Leung, and S. Wong, J. Heat Transfer **120**, 30 (1998).
[36] A. Jain, Y. J. Yu, and A. J. H. McGaughey, Phys. Rev. B **87**, 195301 (2013).
[37] Z. Tian, K. Esfarjani, J. Shiaomi, A. S. Henry, and G. Chen, Appl. Phys. Lett. **99**, 053122 (2011).
[38] P. Martin, Z. Aksamija, E. Pop, and U. Ravaioli, Phys. Rev. Lett. **102**, 125503 (2009).
[39] F. X. Alvarez and D. Jou, Appl. Phys. Lett. **90**, 083109 (2007).
[40] J. Ma, W. Li, and X. Luo, Phys. Rev. B **90**, 035203 (2014).
[41] A. Ward, D. A Broido, D. A Stewart, and G. Deinzer, Phys. Rev. B **80**, 125203 (2009).
[42] D. Li, Y. Wu, P. Kim, L. Shi, P. Yang, and A. Majumdar, Appl. Phys. Lett. **83**, 2934 (2003).
[43] G. S. Doerk, C. Carraro, and R. Maboudian, ACS Nano **4**, 4908 (2010).
[44] V. I. Ozhogin, A. V. Inyushkin, A. N. Taldenkov, A. V. Tikhomirov, G. É. Popov, E. Haller, and K. Itoh, J. Exp. Theor. Phys. Lett. **63**, 490 (1996).
[45] A. V. Inyushkin, A. N. Taldenkov, A..M Gibin, and H-J. Pohl, Phys. Status Solidi **11**, 2995 (2004).
[46] D. G. Onn, A. Witek, Y. Z. Qiu, T. R. Anthony, and W. F. Banholzer, Phys. Rev. Lett. **68**, 2806 (1992).
[47] A. I. Hochbaum, R. Chen, R. D. Delgado, W. Liang, E. C. Garnett, M. Najarian, A. Majumdar, and P. Yang, Nature (London) **451**, 163 (2008).
[48] L. Zeng, K. C. Collins, Y. Hu, M. N. Luckyanova, A. A. Maznev, S. Huberman, V. Chiloyan, J. Zhou, X. Huang, K. A. Nelson *et al.*, Sci. Rep. **5**, 17131 (2015).
[49] A. Jain, J. H. Alan, and A. McGaughey, Comput. Mater. Sci. **110**, 115 (2015).
[50] P. Jiang, L. Lindsay, and Y. K. Koh, J. Appl. Phys. **119**, 245705 (2016).